

Oxide Stability Analysis and Characterization in a Galvannealed Dual-Phase Steel Exhibiting Coating Defects

¹R. Plessinger, ²S. Seetharaman, ³E. De Moor

Advanced Steel Processing and Products Research Center
Colorado School of Mines
1500 Illinois St. Golden, Colorado, USA, 80401
Phone: (303)-273-3624
Email: ¹rplessin@mines.edu
Email: ²sseetharaman@mines.edu
Email: ³edemoor@mines.edu

Keywords: Dual-Phase steel, Galvannealing, Zinc, Coatings, TOF-SIMS, Silicon, Oxidation

INTRODUCTION

As more emphasis is placed on thinner gauges and stronger steel grades for more fuel efficient, and crash-worthy vehicles, corrosion becomes a more important consideration. This demand has led to the development of advanced high strength steel (AHSS) grades such as dual-phase (DP) and transformation-induced plasticity (TRIP) aided steels. To protect these steels from corrosion, a hot-dip galvanizing (HDG) or galvannealing (GA) process is employed. However, alloying with Mn and Si can cause complex surface oxides during annealing, which may result in defects in the zinc coating¹⁻⁸. In order to increase AHSS galvanizability, selective oxidation of alloying elements in DP and TRIP-aided steel needs to be understood. Depending on annealing atmosphere, the mechanism (internal or external) of oxidation can change, as well as the thermodynamic stability of the oxide. Wagner's theory of oxidation enables prediction of the mechanism of oxidation for binary oxide systems⁹. The defects can be present after pickling and fluxing, causing wettability issues during the HDG process. Coating defects may also form or be further exacerbated by the galvannealing operation. For this work, oxidation mechanism predictions were performed using Wagner's theory of oxidation. In the present study a 0.07C-1.9Mn-0.2Si-0.3Cr galvannealed dual-phase steel which exhibited streaking defects in the coating was analyzed. Light optical metallography (LOM) and scanning electron microscopy (SEM) were performed to characterize defects within the galvannealed coating. Static spectra and 3-D profiling using time of flight secondary ion mass spectrometry (TOF-SIMS) was employed. It was found that Mn rich Si containing oxides are present on the steel-coating interface. It does not appear that these oxides affect wettability, however they may have an influence on intermetallic growth during galvannealing. This, combined with an influence from the micro-grooves of the sink roll in the Zn pot, may lead to the streaking defects observed.

EXPERIMENTAL PROCEDURES

Wagner's theory of oxidation, modified by Birks *et al.*, was used to give insight into conditions leading to internal and external selective oxidation within dual-phase steel grades⁹. The investigated parameters are dew point and temperature. The dew point is of interest as it provides an estimation of the oxygen levels that may be available for oxidation reactions based on the H₂O content of a furnace atmosphere. This estimation of water content in the atmosphere is assumed to be in equilibrium with the specified hydrogen content. Oxygen partial pressures can then be calculated. The corresponding oxygen level estimated within the furnace can then give an estimation of the surface concentration of oxygen¹⁰. Using atmospheric information along with solute diffusivity values, external/internal oxidation can be predicted according to:

$$N_B^{(o)} > \left[\frac{\pi g^*}{2\nu} N_O^S \frac{D_O V_m}{D_B V_{ox}} \right]^{1/2} \quad (1)$$

with $N_B^{(o)}$ the concentration of solute metal B within the Fe matrix, in this case B will be Mn, Si or Cr. N_O^S is the surface concentration of oxygen; D_O is the diffusivity of oxygen within the iron matrix, considered for both ferrite and austenite¹¹; D_B is the diffusivity of the substitute solute being oxidized within the Fe matrix; V_m is the molar volume of the metal that is being oxidized, and V_{ox} is the molar volume of the oxide being formed. The critical volume fraction of oxide to cause a change from internal to external oxidation is g^* and it has been suggested to use 0.2 for Mn and 0.3 for the other elements⁷. The atmosphere assumed for analysis was an N₂-5 pct H₂ mixture. Equation 1 acts as a balance between the diffusion of atomic oxygen into the matrix, and diffusion of solute metal to the surface. Depending on concentration, phases and solute species, external, internal and mixed oxidation can occur. If $N_B^{(o)}$ is greater than the product on the right, external oxidation is predicted.

The composition of the analyzed galvanized dual-phase steel is included in Table I. The material was observed to have a streaking style defect. Critical values used for the oxide stability analysis are included in Table II for ferrite and Table III for austenite^{7,10-11}. Additional modeling for thermodynamic stability of oxides was performed using Thermo-Calc®, with the TCFe9 database.

Table I: Chemical Composition of Investigated Material

	C	Mn	Si	Cr	Al	P	S
wt pct	0.07	1.9	0.2	0.3	0.026	< 0.02	< 0.01
atomic pct	0.32	1.9	0.4	0.32	0.05	< 0.04	< 0.02

Table II: Values used in the Wagner Oxide Stability Calculation for Ferrite

Temperature (°C)	D _O (cm ² /sec)	D _{Mn} (cm ² /sec)	D _{Cr} (cm ² /sec)	D _{Si} (cm ² /sec)	g*	g* (Mn)
750	3.84 × 10 ⁻⁷	2.61 × 10 ⁻¹²	1.50 × 10 ⁻¹²	2.40 × 10 ⁻¹²	0.3	0.2
800	6.57 × 10 ⁻⁷	8.93 × 10 ⁻¹²	5.54 × 10 ⁻¹²	8.00 × 10 ⁻¹²		

Table III: Values used in the Wagner Oxide Stability Calculation for Austenite

Temperature (°C)	D _O (cm ² /sec)	D _{Mn} (cm ² /sec)	D _{Cr} (cm ² /sec)	D _{Si} (cm ² /sec)	g*	g* (Mn)
850	8.07 × 10 ⁻⁸	9.38 × 10 ⁻¹⁴	9.00 × 10 ⁻¹⁴	1.02 × 10 ⁻¹²	0.3	0.2
900	1.74 × 10 ⁻⁷	3.13 × 10 ⁻¹³	3.00 × 10 ⁻¹³	3.09 × 10 ⁻¹²		

Characterization of the coating was performed using surface and cross-sectional analysis using LOM and SEM. LOM was performed on an Olympus® SZX12 stereomicroscope, and higher magnification micrographs were taken on a JEOL® JSM-7000 field emission scanning electron microscope. For elemental characterization, the use of an IonToF TOF.SIMS 5 was employed. The analysis on this machine was carried out using a 30 keV, three-lens BiMn cluster ion gun for surface spectra. An oxygen electron impact gas ion source was used for sputtering into the material for 3D characterization. This source is used primarily for analysis of predominantly positive based ions, e.g. metals, but its use limits the analysis of oxides present in the coating. In order to observe the possible oxides formed on the steel surface, a Ce source may also be used. An Ar cleansing process was used prior to each analysis to clean the sample of atmospheric contamination. The information gathered from microscopy and elemental characterization was supplemented with calculations from Wagner's theory of oxidation as well as Thermo-Calc® analysis.

RESULTS AND DISCUSSION

Thermo-Calc® Analysis

Thermo-Calc® analysis was conducted to identify oxide type and to supplement Wagner calculations as well as TOF-SIMS analysis. Table IV shows the relevant stoichiometries of phases as displayed from Thermo-Calc® needed for interpretation of Figure 1. Important oxide species to take into consideration with dual phase or TRIP-aided steels are fayalite (Fe₂(Mn)SiO₄), spinel (Mn(Fe)Cr₂O₄), corundum (M₂O₃) and rhodonite (Mn₂SiO₄). Mn and Si containing oxides are known to cause galvanizability issues within high Mn and Si containing steels¹⁻⁸.

Figure 1 shows the low oxygen content Fe-O phase diagram as created from Thermo-Calc®. The industrially relevant dew points to be taken into consideration range from -30 to 30 °C. The only oxide that is stable for this range of dew points is the corundum phase. This suggests that the Si level in this dual-phase steel is low enough to not form any Si containing oxides on the surface of the steel. However, Mn containing oxides are stable at these dew points. Higher oxygen levels present, *e.g.* in the hot mill or reheating furnace, can result in fayalite and rhodonite formation. If this scale is not fully pickled off, these oxides may decrease galvanizability of dual phase steels²⁻⁹. Another consideration is the thermodynamic deviation of H₂O, which can result in higher quantities of oxidizing gas than estimated by equilibrium H₂ and H₂O levels^{12,13}. Instead of O₂ selectively oxidizing solute, H₂O_(g) can react with solutes to form oxides and hydrogen gas. This will result in different oxides being stable, specifically fayalite and spinel. With the greater additions of Cr (0.6 wt pct) and Mn (1.7 wt pct) to dual-phase steel, it has been shown that a Mn-Cr spinel can form during annealing and can increase wettability of the steel due to its reactivity with Al in the Zn bath (0.14 wt pct Al in Zn)¹².

Table IV: Stoichiometry of Phases from Thermo-Calc®

Phase	Stoichiometry
M6C	(Fe) ₂ (Mo) ₂ (Fe,Si,Cr,Mo) ₂ C
Sigma	(Fe,Mn,Cr,Al) ₁₀ (Cr,Mo) ₄ (Fe,Si,Mn,Cr,Al,Mo) ₁₆
Spinel	(Fe ³⁺ , Fe ²⁺ , Mn ³⁺ , Mn ²⁺ , Cr ³⁺ , Cr ²⁺ , Al ³⁺)(Fe ²⁺ , Mn ²⁺ , Cr ²⁺) ₂ O ₄ ²⁻
Corundum	(Fe ³⁺ , Fe ²⁺ , Mn ³⁺ , Mn ²⁺ , Cr ³⁺ , Cr ²⁺ , Al ³⁺) ₂ (Fe ³⁺ , Cr ³⁺)O ₃ ²⁻
Fayalite	Fe-Mn-SiO ₄
Rhodonite	Mn ₂ SiO ₄

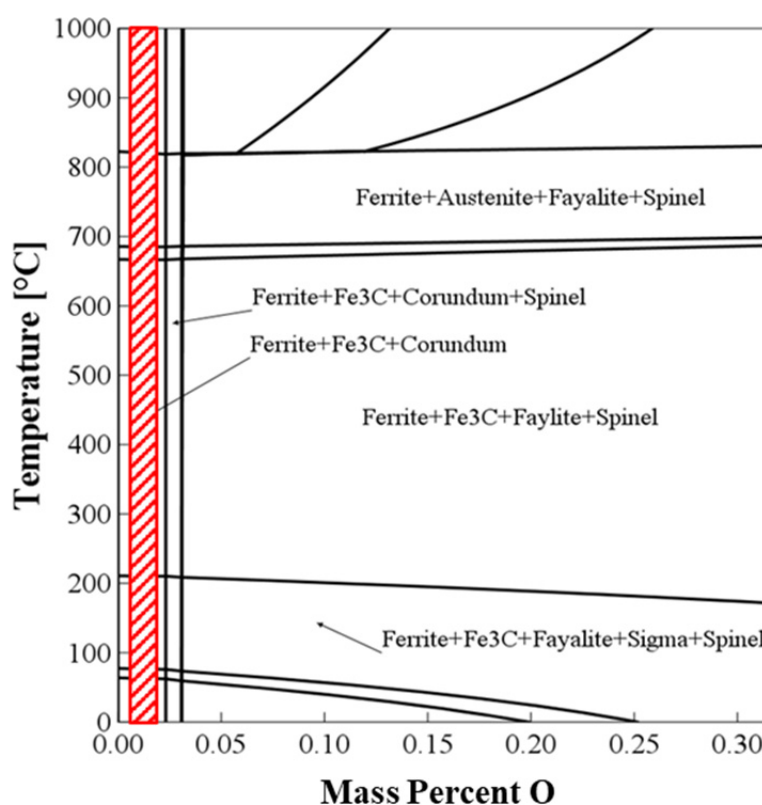


Figure 1: Fe-O phase diagram for investigated material (0.07 C-1.6 Mn-0.2 Si-0.3 Cr-0.026 Al (wt pct)) from Thermo-Calc®. Phases are described in Table IV. The range of relevant dew points is indicated by the shaded area.

Oxide Stability Prediction Using Wagner's Theory of Oxidation

For the prediction of oxidation mechanism, Wagner's theory of oxidation was used for binary oxide systems. Though there is the possibility of complex oxide formation, as indicated by the Thermo-Calc® calculation, this analysis proves useful when looking into the diffusion of solute towards the surface of the matrix. Analyses of both temperature and dew point variation are included for both ferrite and austenite as during intercritical annealing of DP steels, both phases will be present. Using thermodynamic data from the previous section, conclusions will be made about oxide mechanism and stoichiometry. It should be recognized that dew points close to the transition from external to internal oxidation may result in a large amount of error associated with the analysis. Due to this error, both external and internal oxidation should be considered when conditions are close to the transition. Mn, Si and Cr solutes are included in the analysis.

Prediction of Oxide Formation in Ferrite

Figure 2 displays atomic percent of the diffusing solute as a function of dew point (from Equation 1) and effectively shows the transition from internal to external oxidation for Cr, Si and Mn contents within an α -Fe matrix. Higher diffusivity of Cr and Mn is estimated within ferrite versus austenite, increasing the probability of external oxidation at higher dew points. Because Si and Cr diffusivities are greater than Mn diffusivity, these solutes may result in a higher probability of external oxidation. However, it should be noted that recent literature has shown that high Cr levels (0.6 wt pct) can help wettability of molten Zn as Mn-Cr spinel can form externally. This oxide is reactive to Al, resulting in $Mn(Cr,Al)_2O_4$ to form, which in turn can be taken up into the Zn bath, exposing the Fe substrate¹². Cr and Si solute additions are low enough that Wagner's theory predicts that they will internally oxidize in ferrite at industrially relevant dew points (-30 to 30 °C). However, if the oxidizing conditions were to increase, these solutes can oxidize externally at the mentioned dew point levels. Furnace conditions using 5 vol pct H_2-N_2 with an approximate -35 °C dew point atmosphere have shown Mn-Cr spinel formation when Cr levels reach 0.6 wt pct¹². As temperature increases, Mn and Cr show increased probability of external oxidation at higher dew point. Si does not show a temperature dependence.

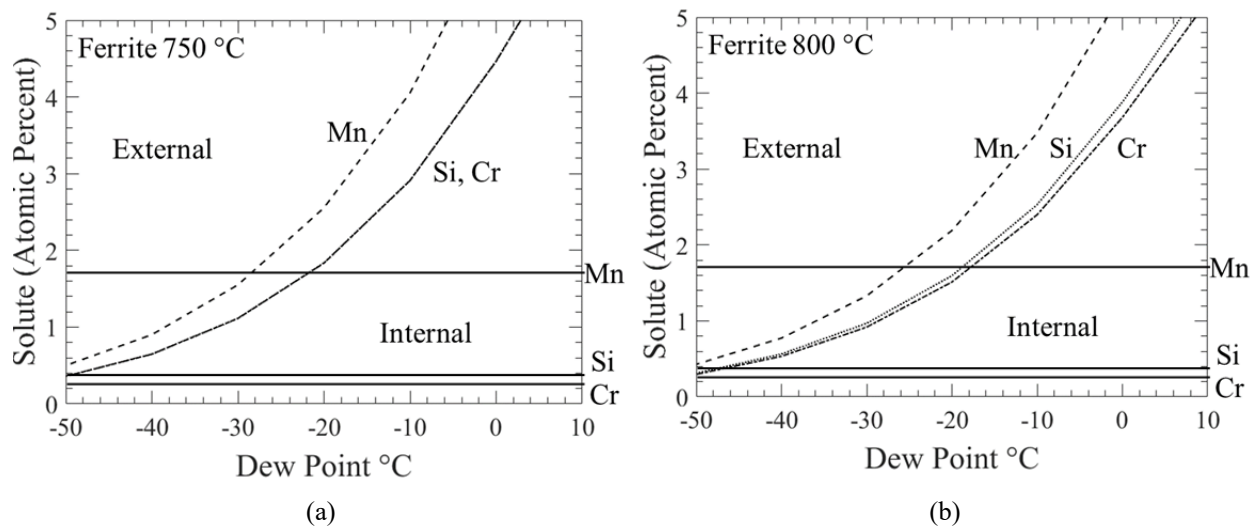


Figure 2: Oxidation mechanism plots derived from Wagner's theory of oxidation. Mn, Si and Cr levels for the investigated steel are indicated on the plot. (a) is for ferrite at 750 °C and (b) is for ferrite at 800 °C.

Prediction of Oxide Formation in Austenite

Calculations from Wagner's theory for austenite are shown in Figure 3. Cr and Mn diffusivities are shown to be lower in austenite than in ferrite, resulting in lower probability of external oxidation at higher dew points. Si diffusion is similar in austenite and ferrite. Increasing dew point and lower temperature results in lower probability of external oxidation. As mentioned in the discussion for ferrite, a Mn-Cr spinel could form at higher oxidizing conditions and may decrease the wetting angle during the galvanizing process. Since the Cr level is at 0.3 wt pct (0.32 atomic pct), the chance for the spinel to form may be less probable as Cr levels in the investigated steel are low enough to predict internal oxidation. Mn and Cr are predicted to internally oxidize at industrially relevant dew points. Si has the probability to externally oxidize at low dew points, however the dew point at which it is probable to externally oxidize is not within industrially relevant dew point ranges. As temperature increases, Mn and Cr have a higher probability of external oxidation at higher dew points, however the increase is only by a few degrees of dew point. Si does not show a temperature dependence in austenite. The substrate phase has a greater effect on oxidation mechanism than temperature, with ferrite having higher probabilities of external oxidation at higher dew points. During hot rolling and the HDG process, it is expected that a large fraction of ferrite will be present on the surface of the steel. This could lead to an increase in external oxidation.

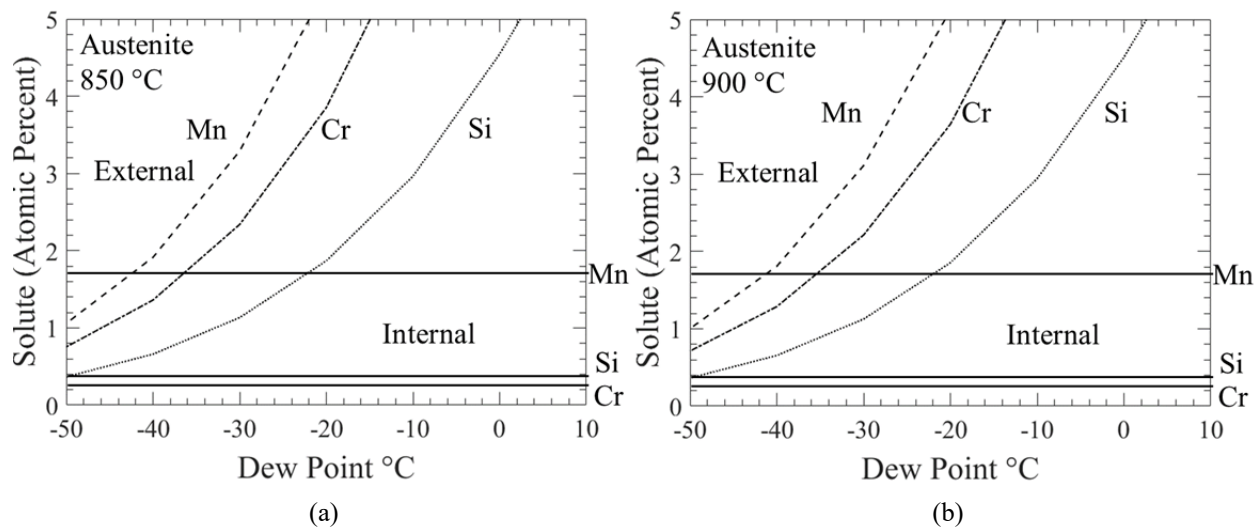


Figure 3: Oxidation mechanism plots derived from Wagner's theory of oxidation. Mn, Si and Cr levels of the investigated material are indicated on the plot. (a) is for austenite at 850 °C and (b) is for austenite at 900 °C.

Experimental Characterization

To compare theoretical calculations with experimental analysis, light optical, scanning electron microscopy and TOF-SIMS were performed.

Microstructural Characterization

Stereomicroscopy and SEM micrographs of the surface of the coating showing streaking defects are observed in Figure 4. Figure 4 (a)-(c) are the same orientation, with the streaks parallel to the rolling direction, vertical in the micrographs. Arrows on Figure 4 indicate areas of defects on the surface. The observed streaks appear to be approximately 2 mm apart. As magnification is increased, smaller streaks on the order of 200 μm become apparent. This suggests that there may be two mechanisms causing the defects. Depressed areas shown in Figure 4 (c) show the presence of cubic delta and rod zeta phase crystals alluding to the possibility that there is an influence on zinc intermetallic formation¹⁴. Delta phase Zn-Fe intermetallic is the second phase to form in the GA process and is a medium Fe content intermetallic (approximately 7-10 wt pct Fe)^{15,16}. There appears to be some macroscopic periodicity to the streaks, shown in Figure 4 (a). This suggests that the sink roll may be influencing the coating growth. This could be by means of degradation of the inhibition layer during galvanizing, which would lead to differences in growth during galvannealing. Sink rolls can exhibit a micro-grooved surface with a 2 mm pitch, which correlates with the periodicity of the observed streaks¹⁶. The micro-grooved surface of sink rolls has shown to have an influence on the formation of the inhibition layer during the coating process. The small streaks visible with SEM exhibit a surface texture indicative of a temper roll. Since some areas exhibit a temper roll finish, and other areas show the presence of delta and zeta crystals, it suggests that the rolled areas are raised. The brighter areas from stereomicroscopy are these raised areas as these areas have a smoother finish, resulting in more light reflection. Dark areas in SEM micrographs indicate areas that are raised above the observed delta crystals. Figure 4 (d) shows a grey scale intensity profile taken from left to right on the micrograph in Figure 4 (b). This shows that the raised area (bright area in Figure 4 (a)) is approximately 1-2 mm wide, consistent with the distance between streaks in Figure 4 (a). Cross-section SEM analysis showed that the GA coating was $15 \pm 2 \mu\text{m}$, and showed areas of large variability, ranging from 13 μm to 22 μm . This would support the idea that certain areas experience growth rate disparities, resulting in the raised areas that were subjected to the temper roll.

TOF-SIMS

TOF-SIMS surface analysis and 3D profiling was performed on a streaking defect. Surface spectra for a streak are shown in Figure 5. Figure 5(a) is a LOM image of the analyzed surface showing a "risen" defect, Figure 5 (b)-(e) are elemental maps of Zn, Mn, Fe, and Si respectively. The defect is shown to be Zn and Fe rich, with the intermediate areas being rich in Mn and Si, though Si is more uniform. Higher Fe content in the streak may suggest formation of delta phase rather than zeta. However, since the TOF-SIMS scales the areas, and delta/zeta phases exist with a specific Fe content range, it is difficult to identify Zn phases with this analysis. 3-D elemental spectra of Mn, Fe and Si on the steel-coating interface are shown in Figure 6. This area is the same streak observed in Figure 5 (a). It should be mentioned that the micron bars in Figure 6 only fit the x-axis, as the y (sputter) axis will be shorter. The TOF-SIMS data software processes the data into a cube after profiling. The sputter depth was not 100 μm , but rather approximately 20 μm and the y-axis has therefore been stretched approximately five-fold.

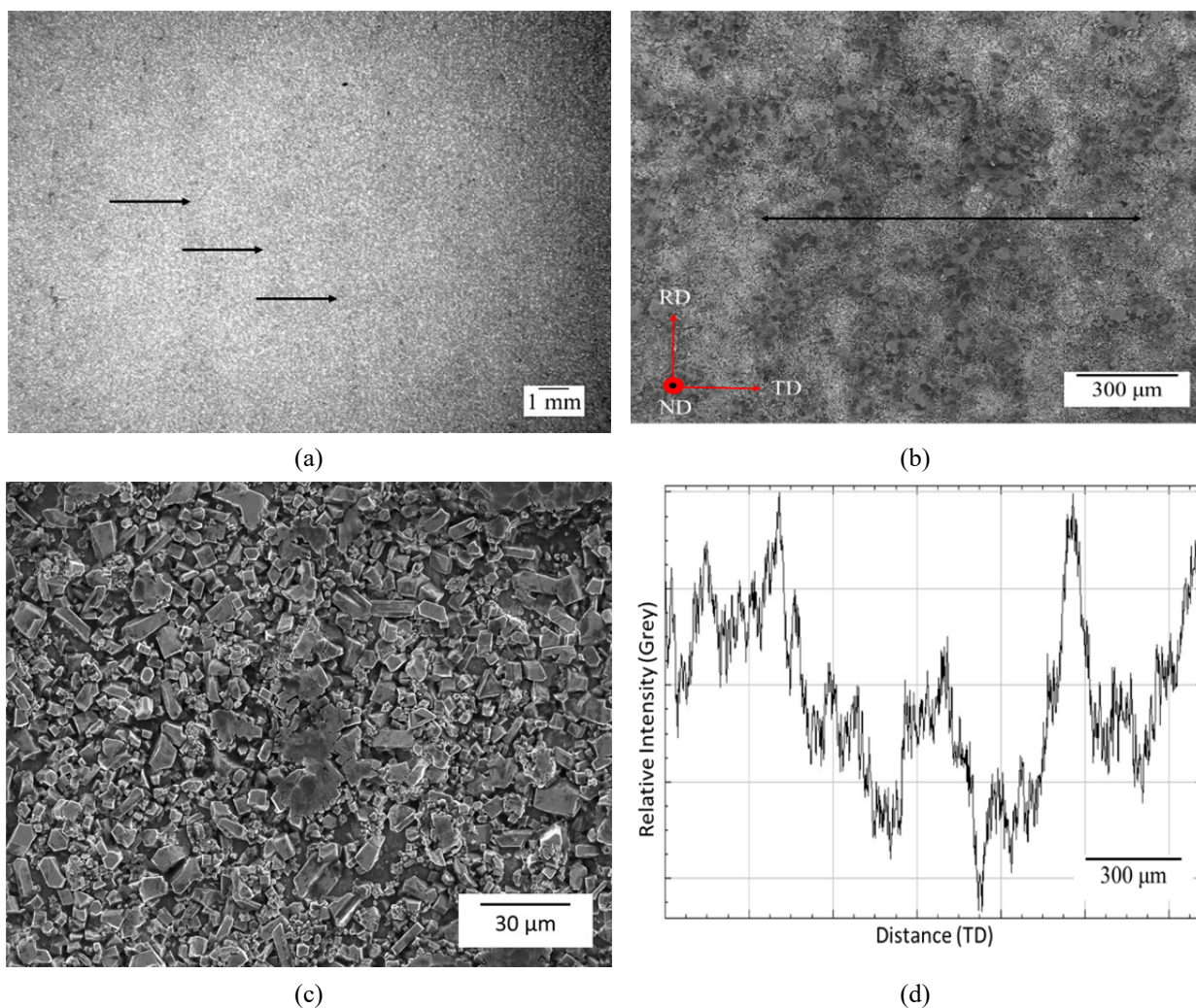
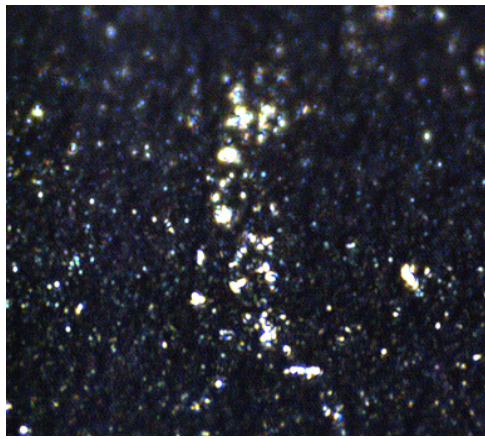


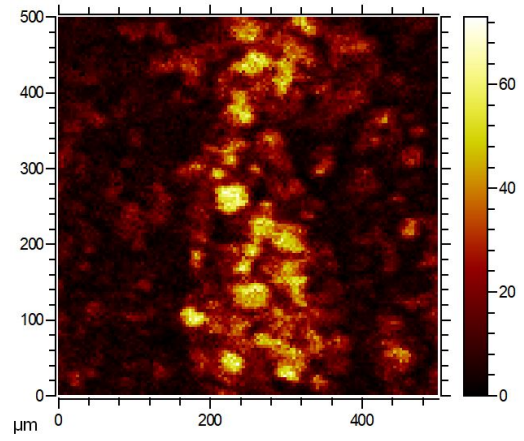
Figure 4: A stereomicroscope image showing galvannealed surface containing defects (a) with streaks indicated, (b) an SEM micrograph of an area showing the streaks. (c) shows an SEM micrograph of delta and zeta phase crystals and (d) a grey scale intensity profile showing the raised area of a surface defect.

Shown in Figure 6 (a) is the cross-sectional information on the Fe distribution from a 3-D depth profile. Seen in this micrograph is the interface between Zn and Fe, with the black regions being the iron deficient regions. There is also some local concentration of Fe in the coating. A higher Fe content suggests that this area may be a different intermetallic species. However, it is observed that Zn is concentrated in these areas as well, shown in Figure 6 (b) where black areas are Zn deficient regions. Since Zn is concentrated to the same area as Fe, this area is not a different phase; rather, this difference could be due to the presence of Mn and Si in the areas where Zn and Fe contents are lower. It should be noted that Si is nearly insoluble in zeta phase, however Si can dissolve to approximately 1 wt pct in delta phase¹⁶. The differences in Si content may suggest that the coating is made up of delta and zeta phase, which is corroborated by surface features¹⁸.

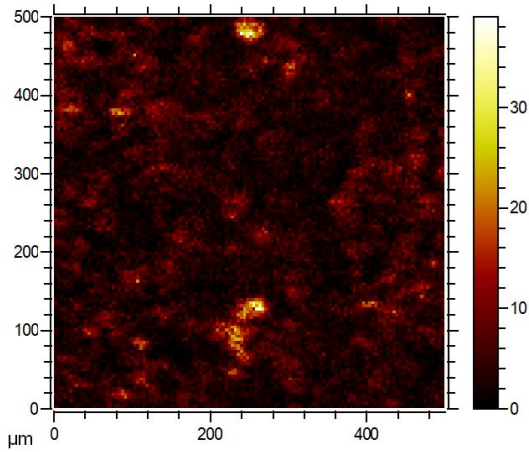
High levels of Mn and Si were detected near the coating-steel interface, shown in Figure 6 (a) and (b). They appear to be globular in nature. This suggests that Mn rich Si containing oxides may be disrupting the formation of the coating. Lin *et al.* suggested that during galvannealing, Si will enrich in a layer just above the steel surface, into the molten Zn¹³. This is postulated through dissolution of Si from the steel, as well as aluminothermic reduction of Si oxides on the surface of the steel. This layer forms as Si solubility in molten Zn is much higher than in Zn-Fe intermetallic phases¹³. Lin suggests that this Si rich layer will suppress intermetallic phase nucleation as well as Fe diffusion into the coating, disrupting galvannealing intermetallic reactions¹³. Since Si solubility is extremely low in zeta phase, nucleation of zeta, as well as growth, would be influenced by the Si content in the steel. In the investigated steel, Si levels are low and Mn levels are high, resulting in a Mn rich defect, with some Si content. The Mn rich, Si containing oxides present on the surface could also influence zeta phase nucleation during galvanizing and subsequent intermetallic galvannealing reactions.



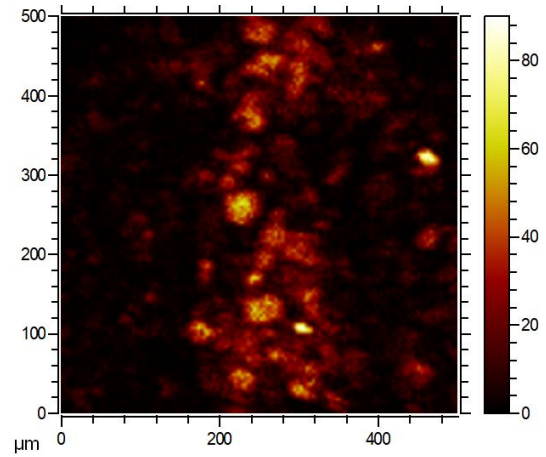
(a) LOM



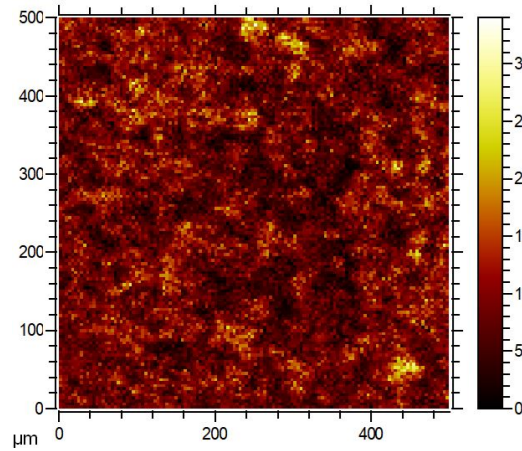
(b) Zn



(c) Mn



(d) Fe



(e) Si

Figure 5: Surface static TOF-SIMS chemical analysis including (a) LOM image of analyzed area (b) Zn map (c) Mn map (d) Fe map and (e) Si map within a surface defect on the investigated material.

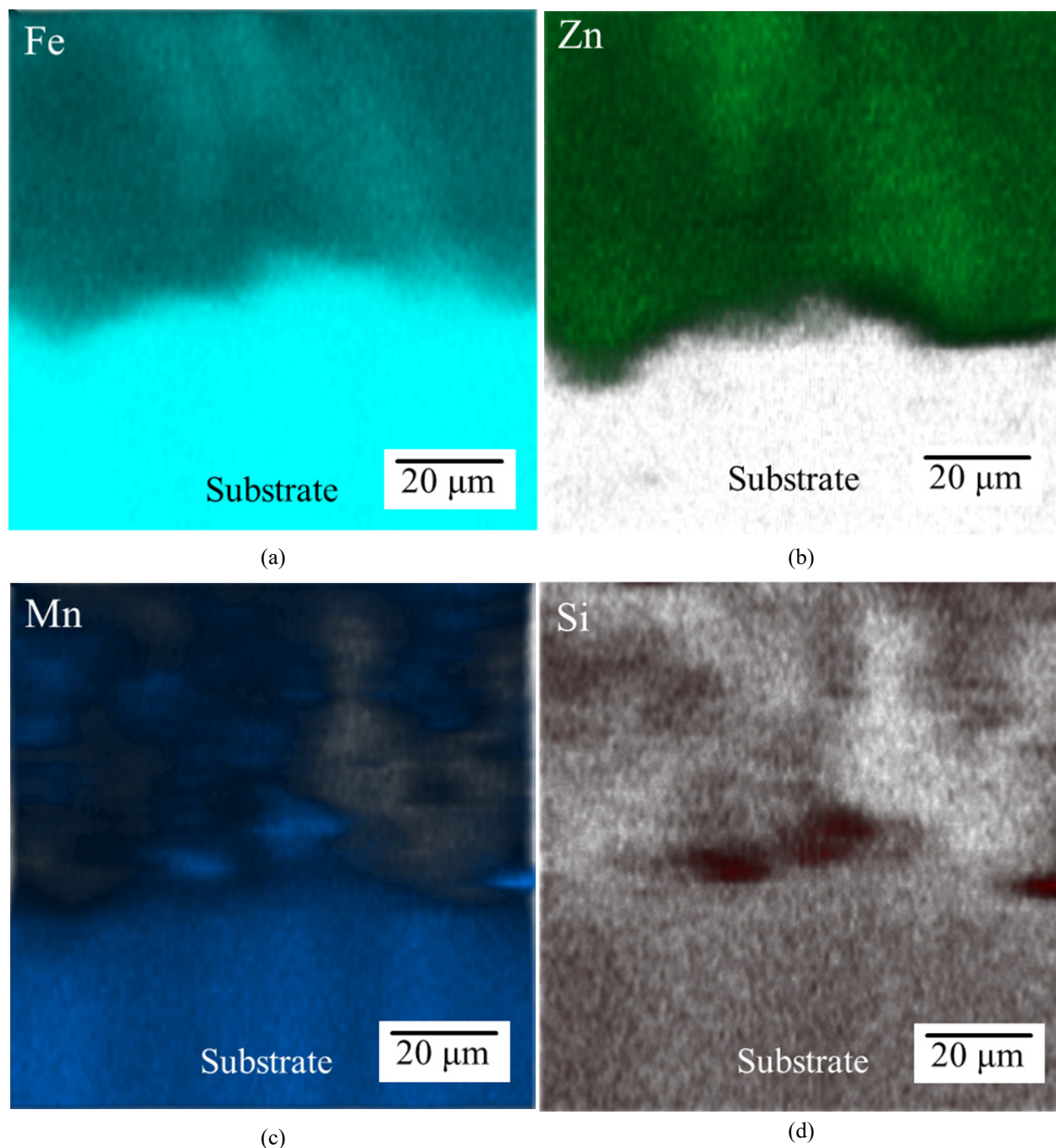


Figure 6: TOF-SIMS cross-sectional chemical analysis (a) Fe map showing Fe diffusion into the coating (b) Zn map showing the absence of bare spots and (c) Mn showing high levels at the steel-coating interface in half spherical arrangement and (d) Si map showing high levels at the steel-coating interface in half spherical arrangement

Referring to Wagner's theory of oxidation, Mn is predicted to externally oxidize within industrially relevant dew point ranges. However, there is also the presence of Si within the oxides, which was predicted to oxidize internally. This could be due to the large amount of error associated with using Wagner's theory of oxidation to estimate oxidation mechanism. Estimations of diffusion and the g^* value could result in large enough error that external oxidation could be probable when internal oxidation is the only mechanism predicted. This type of analysis also does not take complex oxides into account, which could be the reason for Si content within the observed oxides. Another variable assumed when estimating oxidation mechanism is that O_2 is the only oxidizing gas in the annealing furnace. It has been suggested that H_2O could behave as O_2 , and since it is at a higher partial pressure than O_2 , H_2O could be the main oxidizing gas¹³. Higher oxidizing potentials make different oxides stable, like spinel, rhodonite and fayalite, shown in Figure 1. Fayalite has been shown to coat grain boundaries, and without proper pickling, can lead to issues with galvanizability^{1-8,18}. However, TOF-SIMS analysis on cold

rolled full hard uncoated dual-phase steel showed uniform elemental distributions, suggesting that Mn-Si oxides formed during annealing. Mn and Si surface spectra for cold rolled full hard uncoated material are shown in Figure 8.

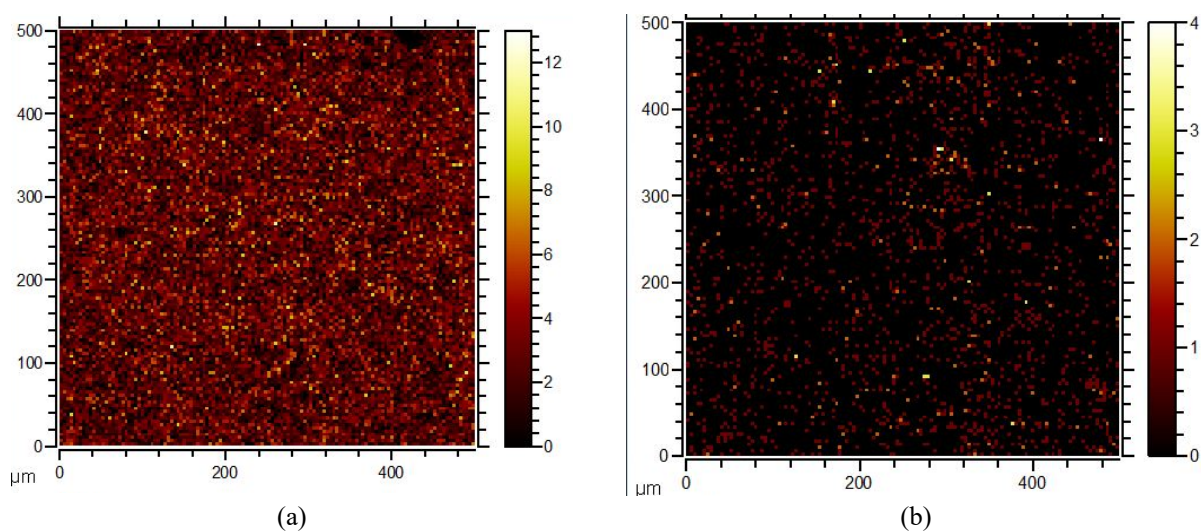


Figure 8: TOF-SIMS surface spectra for (a) Mn and (b) Si on the cold rolled full hard dual-phase steel. Elements are shown to be uniformly distributed.

CONCLUSIONS

A galvanized dual phase steel exhibiting streaking defects was analyzed using microscopy (LOM and SEM), TOF-SIMS analysis, and oxide stability analysis using Thermo-Calc® and Wagner's theory of oxidation calculations were performed.

- It was found from Thermo-Calc® analysis that corundum (M_2O_3 with M being Mn, Cr, or mixed) is the only stable oxide phase that should be present during annealing at industrially relevant dew points.
- Calculations derived from Wagner's theory of oxidation showed that ferrite has a higher susceptibility to external oxidation than austenite. Cr and Si were found to internally oxidize for industrially relevant dew points in ferrite and austenite, and Mn was found to externally oxidize at low industrially relevant dew points ($-25\text{ }^\circ\text{C}$) in ferrite.
- SEM and LOM found that the streaking defects appear to have macroscopic periodicity (1-2 mm) and have raised areas that have a temper rolled surface finish. The intermediate areas appear to have cubic delta and rod-like zeta phase crystals.
- TOF-SIMS 3D-profiling analysis shows the presence of globular particles on the surface of the steel, underneath the Zn coating. These particles are thought to be Mn rich Si containing oxides. Mn oxidation agrees with Wagner calculations and Thermo-Calc® analysis. It is suggested that the oxides do not disrupt wettability due to the absence of bare spots in the coating.
- Due to the periodicity of the streaking defects, and no observed bare spots, it is thought that there are two mechanisms that could be influencing the creation of defects: the Zn pot sink roll micro-grooved surface degrading the inhibition layer formed in the Zn bath, and Mn rich, Si containing oxides influencing formation of the inhibition layer, as well as intermetallic growth, influencing coating thickness.

ACKNOWLEDGMENTS

The support of the International Zinc Association (IZA) and the sponsor of the advanced steel processing and products research center (ASPPRC) at the Colorado School of Mines is gratefully acknowledged. Frank Goodwin with the IZA is gratefully acknowledged for his support and technical input. This material makes use of the TOF-SIMS system at the Colorado School of Mines, which was supported by the National Science Foundation under Grant No.1726898. The authors would like to acknowledge Michael Walker at the Colorado School of Mines for his help with TOF-SIMS data acquisition.

REFERENCES

1. J. Mahieu, J. Maki, B. C. De Cooman, and S. Claessens, "Phase Transformation and Mechanical Properties of Si-Free CMnAl TRIP-Aided Steel," *Metallurgical and Materials Transaction A*, vol. 33, 2002, pp. 2573-2580.
2. H. Liu, Y. He, and L. Li, "Application of Thermodynamics and Wagner Model on Two Problems in Continuous Hot-Dip Galvanizing," *Applied Surface Science*, vol. 256, no. 5, 2009, pp. 1399-1403.
3. B. C. De Cooman, J. Oh, L. Cho, and C. Lee, "Surface Selective Oxidation, Hot-Dip Galvanizing and Coating-Related Properties of Advanced High-Strength and Ultrahigh-Strength Automotive Steel Grades," *Iron and Steel Technology*, vol. 14, no. 2, 2017, pp. 76-79.
4. J. Mahieu, S. Claessens, B. C. De Cooman, and F. Goodwin, "Surface and Sub-Surface Characterization of Si-, Al- and P-Alloyed TRIP-Aided Steel," *Galvatech '2004: 6th International Conference on Zinc and Zinc Alloy Coated Steel Sheet*, Chicago, IL: Association for Iron and Steel Technology, 2004, pp. 529-538.
5. S. Il-ryoung, K. Jong-sang, and S. Seetharaman, "Effect of Dew Point and Gas Flow Rate on the Surface Oxidation of Advanced High Strength Steels," *ISIJ International*, vol. 55, no. 9, 2017, pp. 2008-2017.
6. C. Thorning and S. Sridhar, "Grain Boundary Ridge Formation During Initial High Temperature Oxidation of Mn/Al TRIP Steel," *Philosophical Magazine*, vol. 87, no. 23, 2007, pp. 3479-3499.
7. Y. F. Gong, S. Biroasca, H. S. Kim, and B. C. De Cooman, "Oxide Formation and Alloying Elements Enrichment on TRIP Steel Surface During Inter-Critical Annealing," *Journal of Microscopy*, vol. 230, no.3, 2008, pp. 424-434.
8. B. C. De Cooman, J. Oh, L. Cho, and C. Lee, "Surface Selective Oxidation, Hot-Dip Galvanizing and Coating-Related Properties of Advanced High-Strength and Ultrahigh-Strength Automotive Steel Grades," *Iron and Steel Technology*, vol. 14, no. 2, 2017, pp. 76-79.
9. N. Birks, G.H. Meier, and F.S. Pettit, "Oxidation in Alloys," *Introduction to the High Temperature Oxidation of Metals*, Cambridge University Press, Cambridge, N.Y., 2006, pp. 104-115.
10. J. H. Swisher and E. T. Turkdogan, "Solubility, Permeability, and Diffusivity of Oxygen in Solid Iron," *Transactions of the Metallurgical Society of AIME*, vol. 239, no. 4, 1967, pp. 426-431.
11. D. Huin, P. Flauder, and J. B. Leblond, "Numerical Simulation of Internal Oxidation of Steels During Annealing Treatments," *Oxidation of Metals*, vol. 64, 2005, pp. 131-167.
12. Y. Fushiwaki, T. Kawano, and Y. Nagataki, "Influence of Cr Addition on Selective Oxidation Behavior of Mn-Added High-Strength Steel Sheet," *ISIJ International*, vol. 58, no. 9, 2018, pp. 1623-1628.
13. K. Lin and C. Lin, "Effect of Silicon in Dual Phase Steel on the Alloy Reaction in Continuous Hot-dip Galvanizing and Galvannealing," *ISIJ International*, vol. 54, no. 10, 2014, pp. 2380-2384.
14. S. Sriram, V. Krishnardula, and H. Hahn, "Influence of Delta Phase Morphology in Galvannealed Coated Steels on Formability," *IOP Conference Series: Materials Science and Engineering*, no. 418, pp. 1-9, 2018.
15. A. R. Marder, "The Metallurgy of Zinc-Coated Steel," *Progress in Material Science*, vol. 45, 2000, pp. 191-271.
16. H. H. Fukubayashi, "Present Furnace and Pot Roll Coatings and Future Development," *Galvanizers Association*, Indianapolis, 2001.
17. K. Lin, P. Chu, C. Lin and H. Chen, "Galvanizing and Galvannealing Behavior of CMnSiCr Dual-Phase Steels", *Metallurgical and Materials Transactions A*, vol. 44A, 2013, pp. 2690-2698
18. R. Y. Chen and W. Y. D. Yuen, "Examination of Oxide Scales of Hot Rolled Steel Products," *ISIJ International*, vol. 45, no. 1, 2005, pp. 52-59